Hindawi
Mobile Information Systems
Volume 2022, Article ID 5017000, 11 pages
https://doi.org/10.1155/2022/5017000

Research Article

Retrieval Algorithm of Water Pollutant Concentration Based on UAV Remote Sensing Technology

Min Ling,[1] Qun Cheng,[1] Jun Peng,[2] Ling Jiang,[2] and Ruifeng Wang[3]

[1]*Shanghai Urban Construction Engineering School (Shanghai Gardening School), Shanghai 200232, China*
[2]*School of Geographic Information and Tourism, Chuzhou University, Chuzhou 239000, China*
[3]*Shanghai Urban Construction Vocational College, Shanghai 200438, China*

Correspondence should be addressed to Jun Peng; pj_0519@chzu.edu.cn

Received 4 January 2022; Revised 23 February 2022; Accepted 28 February 2022; Published 30 April 2022

Academic Editor: Mukhtaj Khan

With the development of the society and economy, traditional water pollution monitoring methods can no longer meet the normal needs of work. Unmanned aerial vehicle remote sensing technology has gradually emerged, and it has shown a development trend of multimodel and multifunction. However, the application of UAV remote sensing technology in water pollution monitoring is in its infancy and has not formed a unified method and standard. This paper introduces the disadvantages of UAV Remote Sensing Technology in water pollution monitoring and provides a way to improve the application level of UAV Remote Sensing Technology in water pollution monitoring. In order to make full use of the advantages of remote sensing monitoring technology in water ecological environment monitoring, including wide coverage, fast analysis speed, accurate and reliable monitoring results, and large amount of information, according to the spectral effect of polluted water, a remote sensing inversion model of river and lake parameters is established to determine the water quality of rivers and lakes. Concentrations of pollutants in the body are inverted and analyzed. The analysis results show that the fitting effect of the inversion model is accurate and the accuracy errors reflected by the degree of dispersion and deviation are also acceptable. The inversion results of the concentration of river and lake characteristic parameters based on the Gaofen-1 remote sensing image data are in line with the actual situation. The research results can greatly strengthen the monitoring capacity of the sewage outlet and provide reference for related research on water pollution caused by the sewage outlet.

1. Introduction

With the rapid development of social economy, the ecological environment is deteriorating and environmental pollution problems are becoming more and more serious and sudden environmental pollution accidents occur frequently in industrial production activities. In particular, the raw materials, by-products, and toxic and hazardous materials in the production, storage, and transportation all have a major risk of sudden pollution accidents. Therefore, in order to minimize environmental pollution and ecological damage, protect people's lives and property, and promote sustained and stable economic development, it is necessary to establish a fast and efficient early warning and emergency response system and accident rescue mechanism and do a good job in the investigation and prevention of sudden environmental pollution accidents.

1.1. Early Warning and Forecasting and Processing Work. Sudden environmental pollution accidents are different from general environmental pollution. There is no fixed discharge method and discharge route. They are vicious accidents that occur suddenly and are difficult to control, discharge large amounts of pollutants in a short period of time, and cause

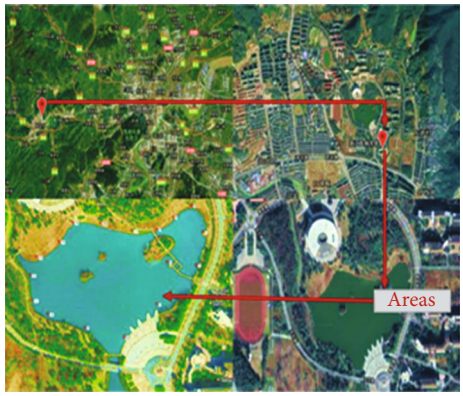

Figure 1: Experimental area sampling points.

heavy losses to people's lives and property. Sudden environmental pollution accidents can be divided into five types according to the nature of the pollutants and the way in which they occur: leakage and diffusion of highly toxic pesticides and toxic chemicals, oil spills, pollution incidents caused by the leakage of flammable and explosive substances, and urban sewage and factories and mines.

1.2. Irregular Discharge of Wastewater and Nuclear Pollution Accident. Among them, sudden water pollution accidents caused by the discharge of a large amount of abnormal waste water occur most frequently. Sudden water pollution accidents are mostly caused by waterway traffic accidents, illegal discharges by enterprises or accidental discharges, and pipeline ruptures. Uncertainty is the most important feature of sudden water pollution accidents [1–3]. Even if basic information such as the time and location of the accident and the nature of the accident water area are obtained through on-site surveys, the type and quantity of pollutants discharged are difficult to determine due to the time lag in the discovery of pollution accidents. These data are exactly what is needed for water environment simulation analysis.

1.3. Basic Parameters. In addition, pollution accident information is also incomplete and incomparable. Although water pollution accidents have occurred frequently, the full process information of a typical pollution accident has not yet been obtained. Based on the abovementioned analysis, due to the time, location, process, scale of the sudden water pollution accident, the uncertainty of the water area, and the incompleteness of the pollution accident information, it brings accurate simulation and analysis of sudden water pollution accidents and it is quite technically difficult.

The consequences of major sudden water pollution accidents are catastrophic. Once a water pollution accident occurs in the upper reaches of the river, the biggest damage will be the urban and rural water supply systems and the water ecological environment along the downstream. In order to prevent the occurrence of sudden water pollution accidents and minimize the extent and scope of pollution accidents that have occurred, it is quite necessary to establish an early warning and emergency system for sudden water pollution accidents [4–8].

For the early warning and emergency work of water pollution accidents, the migration of the pollution zone and the temporal and spatial changes of the concentration through on-site monitoring are far from meeting actual needs. On the one hand, there are limited sections for on-site monitoring and can only determine the current pollution status of the polluted river and cannot scientifically and quantitatively predict the development trend of the pollution zone; on the other hand, it cannot make changes in various hydrological parameters and the effects of different control strategies.

1.4. Perform Simulations and Comparisons. Using the mathematical model of water quality to simulate and calculate the water quality and grasp the temporal and spatial changes of pollutant concentration can provide powerful technical support for the water quality prediction of sudden water pollution accidents. Therefore, the accident simulation and prediction system with the water quality mathematical model as the core is the key link to provide early warning and forecast and take correct emergency measures for vulnerable areas. Mathematically, the problem of determining the mathematical model of water quality and its parameters, using the time series of pollutant cross-section concentration as the model boundary condition or source term, and calculating the time and space change process of the pollutant group are called the water quality simulation problem [9, 10].

Due to the sudden nature of water pollution accidents, it is generally difficult to monitor the complete source discharge history in time. It is also difficult to find out the location of the pollution source in time for some accidents caused by industrial enterprises. Therefore, the pollution source information necessary for model calculation is incomplete or uncertain and general water quality mathematical models cannot complete the water quality simulation of sudden pollution accidents. However, the concentration time series data obtained at the downstream observation points of the pollution source can be input into the water pollution accident inversion model to calculate the location of the pollution source and its discharge process and quantitatively determine the responsibility of the unit that caused the accident discharge. Mathematically, the problem of calculating the pollution source emission history from the concentration time series data at the monitoring section is called the water quality simulation inversion problem [11].

In order to be able to scientifically select and decide on emergency measures and achieve effective management of the urban drinking water source water environment, the water quality mathematical model used for the simulation of sudden water pollution accidents needs to meet the following requirements: (1) it has a faster convergence rate and can quickly make predictions through simple operations; (2) it has good calculation stability and can use the input data with a higher level of error to obtain reasonable results; (3) it can adapt to various geographical and hydrological conditions and can simulate and predict the effects of various emergency measures; (4) it has certain parameter insensitivity and can deal with the problem of model

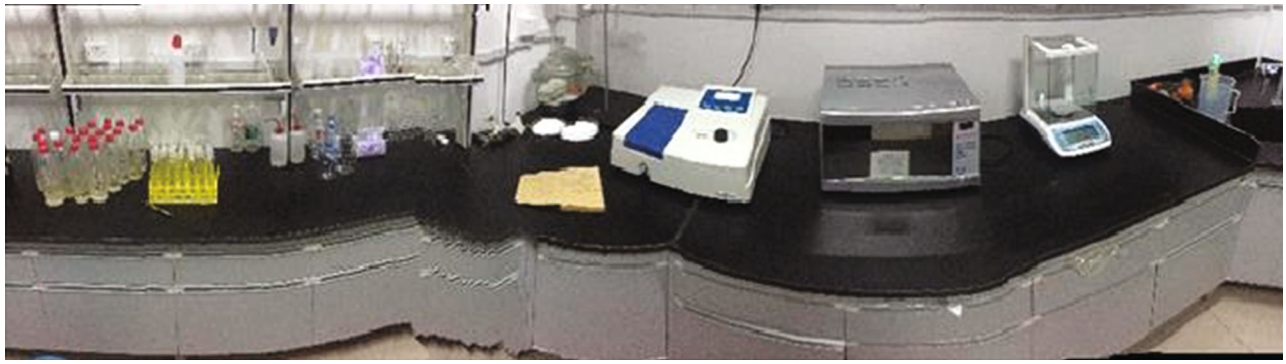

Figure 2: 2.4 hint of lab test of TP.

Table 1: Parameters of TUB.

Test parameters	TUB	SS
Range	0–200 NTU	0–500 mg/L
Error	<±2.5%	<±5.0%
Repeat	<1.0%	<6%
Max	—	<20 W
Environment	5–35°C	5–40°C, <85%
Size	—	310 mm*230 mm*150 mm
Weight	<3 kg	<1.3 kg

parameter calibration due to lack of data; and (5) the calculation results can be visualized, such as visual expression of polluted water bodies with GIS technology [12–16].

The control and planning of river water quality can also be attributed to the problem of inverting the initial distribution of pollutant concentration based on known final concentration data. Huang et al. applied the Tikhonov regularization method and finite difference method to give a numerical method for solving the inverse problem of one-dimensional unsteady turbulent diffusion initial conditions; Pan et al. used the Fourier analysis theory to study the inverse problem of the convection-diffusion equation. The stability of the two-dimensional convection reaction-diffusion equation is decomposed into a series of well-posed forward problems and an ill-posed linear algebraic equations; the classical Euler difference scheme and truncated singular value decomposition method are used to solve forward problems and ill-conditioned equations; the adjoint assimilation method is used to solve the inverse problem of the convection-diffusion equation inverse process [17].

With the continuous development of drone technology, this problem has a brand new solution. UAV remote sensing itself has the advantages of flexible maneuverability, easy operation, high resolution, high timeliness, and low investment cost. UAV remote sensing can be used anytime and anywhere and can bring a lot of data. It provides more convenience for the analysis and prediction of water pollution. It can develop targeted monitoring programs based on the characteristics of the monitored water area and discover some traditions in time.

1.5. Pollution That Is Difficult to Take into Account by the Method. At the same time, it also circumvents the limitation of timeliness of satellite remote sensing. When the weather conditions permit, remote sensing can be carried out on the water area at any time and the water quality changes in the area of interest can be grasped at any time. This is very important for the water quality environmental monitoring of small and microwater areas.

1.6. Significance. This article will rely on UAV remote sensing technology to carry out research on the inversion of pollutant concentration in water bodies [18–20].

In general, the research on the concentration of water quality elements has become a hot topic and there is a wide range of options in the establishment of the inversion model and the selection of remote sensing data, which can be proved by a large number of experiments. At the same time, general inversion models are only valid for the experimental area and specific experimental time period and cannot be widely used in all waters. This is related to the complex characteristics of the second type of water body. Therefore, the experiment is generally aimed at different experimental areas. According to the different seasons to establish and discuss the time-space model. In the past experiments, most of the satellite remote sensing images were used. Such research is mainly aimed at the water color elements of large water areas, and its application is also limited. In this research, the main consideration is to select UAV remote sensing images to obtain higher-precision image data. Through continuous optimization of the algorithm, more accurate inversion results can also be obtained.

The remaining structure of this paper is as follows: Section 2 introduces UAV technology, Section 3 introduces remote sensing technology and its data processing methods, Section 4 throws light on the concentration inversion model, and Section 5 is about summary and prospects.

2. UAV Remote Sensing Technology

With the continuous development of remote sensing technology, there are more and more water quality elements that can be monitored by remote sensing. Except for some large pollution accidents such as thermal pollution of water bodies and oil spill pollution, the water quality elements can be

Figure 3: Detectors and turbidimeter.

Table 2: OL1 land imager.

Band name	Range_low	Range_high	Space resolutions
Coastal	0.433	0.453	30
Blue	0.450	0.515	30
Green	0.525	0.600	30
Red	0.630	0.680	30
NIR	0.845	0.885	30
SWIR1	1.560	1.651	30
SWIR2	2.100	2.300	30
Pan	0.500	0.580	15
Cirrus	1.360	1.390	30

inverted and monitored under daily conditions. The common ones are as follows: (1) suspended sediments concentration (SS), turbidity (turbidity (TUB)), and other related water quality data. The composition of the water environment is complex; various sediments and solid particulate matter with shapes, usually a large number of clay particles, organic debris, plankton, etc., will affect the suspended solid concentration; (2) the influence of aquatic plants on water quality factors, including some common aquatic plants and algae aquatic plants. The water quality factors related to such plants mainly include chlorophyll (chlorophy (Ch1)) and brown pigment (phaeo-pigment). In general, chlorophyll is present in most aquatic plants. In general water quality remote sensing research, the content of chlorophyll a (chlorophy-a (Chl-a)) is used to reflect the content of aquatic plants in the water body; (3) dissolved organic matter (dissolved organic carbon (DOM)). Due to the metabolism of various organisms, a large amount of dissolved organic matter will be produced in the water body, which mainly includes a large amount of organic matter such as particulate organic carbon (POC) and also some colored ones. Dissolved organic matter will flow through forests, swamps, and other complex forest environments in the natural environment, will absorb the blue light from the hjc light, and at the same time scatter the yellow light, making the entire water environment appear pale-yellow, which is a large amount of water quality remote sensing yellow substances in the research; and (4) chemical water quality indicators. These indicators can be divided into two types: aerobic balance indicators and nutritional indicators. Aerobic balance indicators generally monitor the chemical oxygen demand (chemical oxygen demand (COD)) etc. Nutritional indicators are generally monitored for the total nitrogen (TN), total phosphorus (TP), etc. [21–25].

In recent years, research on remote sensing inversion models has continued to increase and the methods and principles of establishing inversion models have also been continuously sublimated. There are endless researches on improving the accuracy of experimental inversion from various angles. Cao used HJ-IA/IB remote sensing imagery in 2012 to conduct Pearson correlation analysis between his total nitrogen and total phosphorus data and remote sensing data using Dianchi Lake as the research area. After selecting the data with higher correlation, the multiple linear regression model, BP neural network, and RBF network model were established. Through comparison, it is found that the artificial neural network model has higher inversion accuracy. Gao et al. first divided Chaohu Lake in 2015. According to the experimentally divided areas, they established multiple linear models for inversion research. The experimental accuracy is high, but the inversion process is more cumbersome due to the division of regions. In 2014, Wang used Hulun Lake as the research area and used MODIS data to establish a remote sensing inversion model of total nitrogen and total phosphorus and inverted the distribution of total phosphorus in Hulun Lake. The nutritional status was studied. In 2016, Zhang and others took Wuliangsuhai as the research area and used MODIS data to conduct remote sensing monitoring of the area. They established polynomial inversion models of total nitrogen and total phosphorus, and the correlation coefficients of the built models were higher than 0.60. In 2005, Du and others used Taihu Lake as the research area and used GOCI remote sensing images to invert the distribution of total phosphorus (TP) in the Taihu Lake area through regression analysis. The accuracy of the model was as high as 0.898 and proved that there are differences in total phosphorus concentration in different

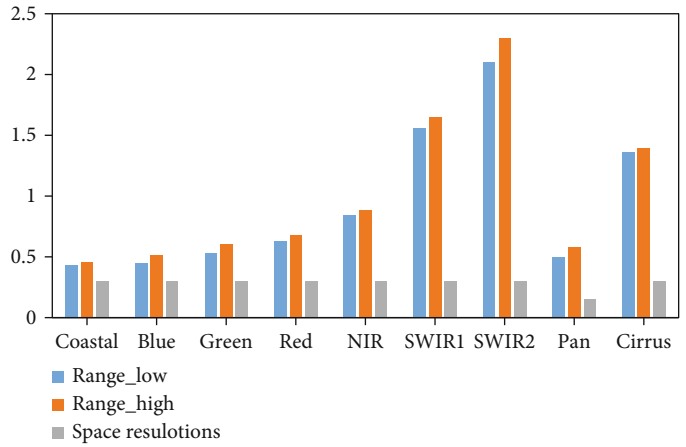

Figure 4: The features of different bands.

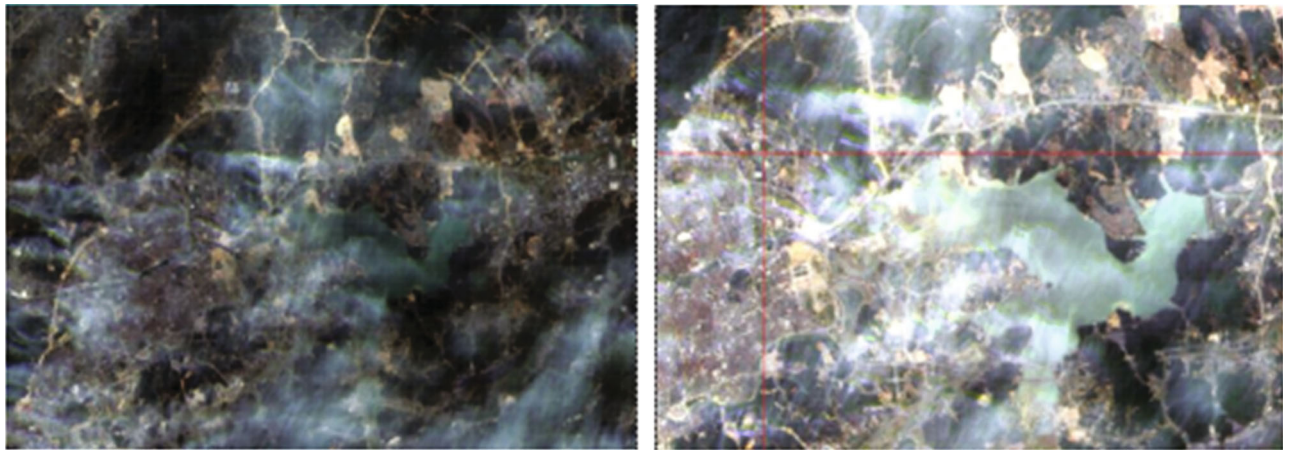

Figure 5: Comparison of cutting images before and after atmospheric correction.

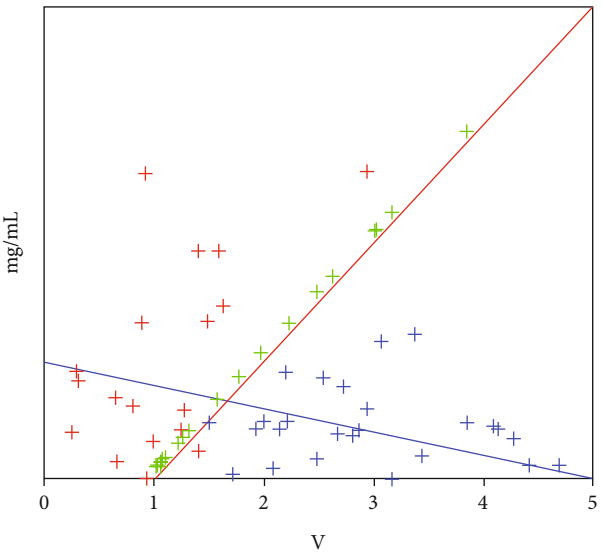

Figure 6: TP significant data.

seasons. But there are similarities in the changes in total phosphorus within a day.

It can be known from many documents that the remote sensing inversion model of water pollutant concentration is mainly empirical and semiempirical. In order to improve the accuracy, the abovementioned regression method will be used. For different seasons, different lakes, and different types of water bodies, there is in general agreement with the highly correlated spectral bands. However, the models established at that time all showed great differences due to differences in time and space. The highest correlations achieved are also not the same, so it is necessary to establish a remote sensing monitoring and inversion model suitable for the pollution concentration of the study area targeted by this study [26–29].

3. Research Area Data Collection and Processing

3.1. Water Quality Sampling. The sampling tool used in this experiment is a cup-type fixed-depth water quality sampler. The instrument is made of stainless steel and will not

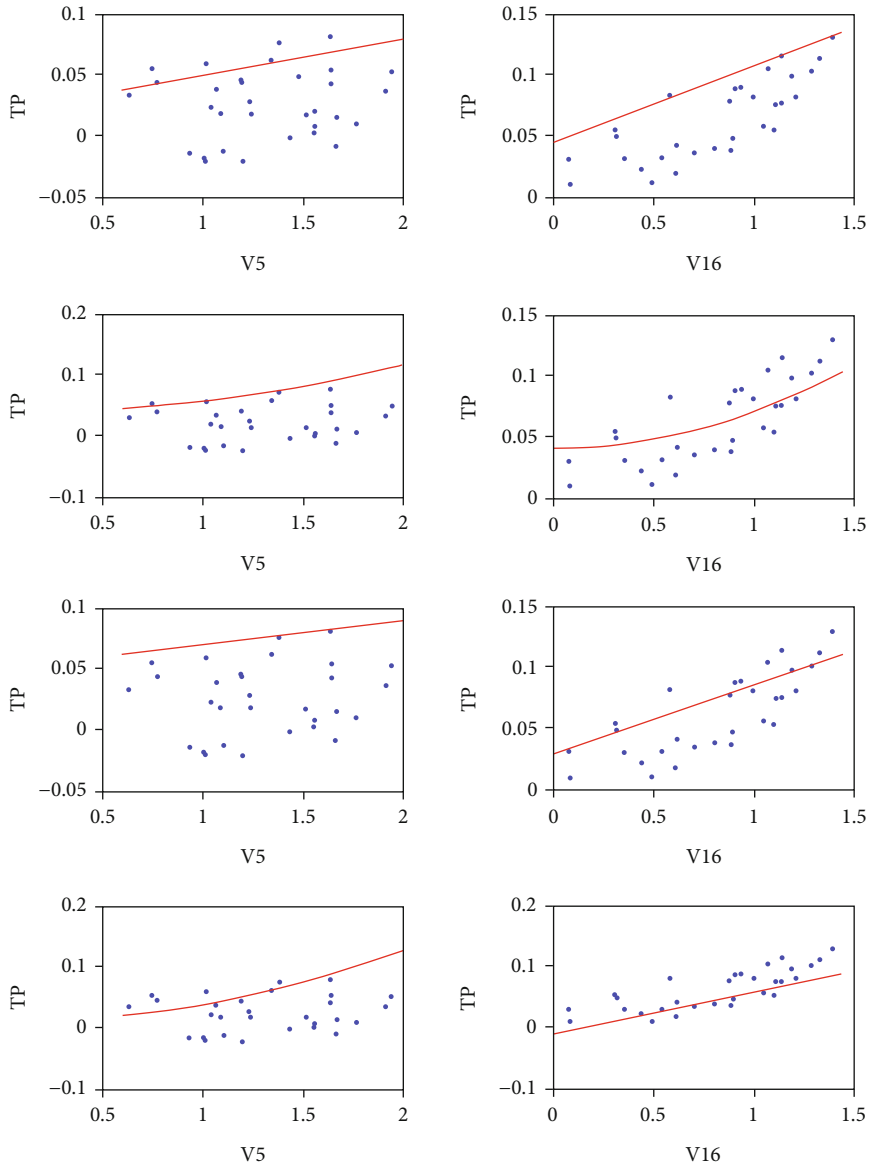

Figure 7: Total phosphorus (TP) inversion model fitting map.

produce a scale and will not chemically react with the sample to affect the nature of the sample. The instrument is compressed by the instrument during use. The top handle keeps the tail cup container closed. In this state, it is 0.5 m deep from the sampling point to the water surface (the length of the purchased instrument is 1 m, and the 0.5 m mark can be marked on the rod before the experiment), after reaching the sampling position. Lift the handle at the top of the instrument and open the top cover of the cup container, so that the water in the sampling area flows into the cup container. After the container is full, continue to seal the container according to the same method, take out the water surface and put the sample into the preprepared sample. Clean well the mineral water bottles, and mark them according to the order of sampling points. Experimental area sampling points are shown in Figure 1.

In this study, water samples were taken with a cup-type fixed-depth water quality sampler in the experimental area four times. The locations of the sampling points are shown in Figure 1. In the process of research, it was discovered that the outlet and inlet are the main factors affecting the spatial distribution of water quality elements in small waters and the experimental waters are regularly drained, so the difference in water quality between the center of the water and the shore is not significant. In summary, in order to facilitate the experiment, only water sampling points are distributed on the shore. There are 20 sampling points for a single experiment, and 500 ml water samples are collected at each point.

3.2. Measured Data of Water Quality Parameters. For the detection of total phosphorus, the platinum antimony

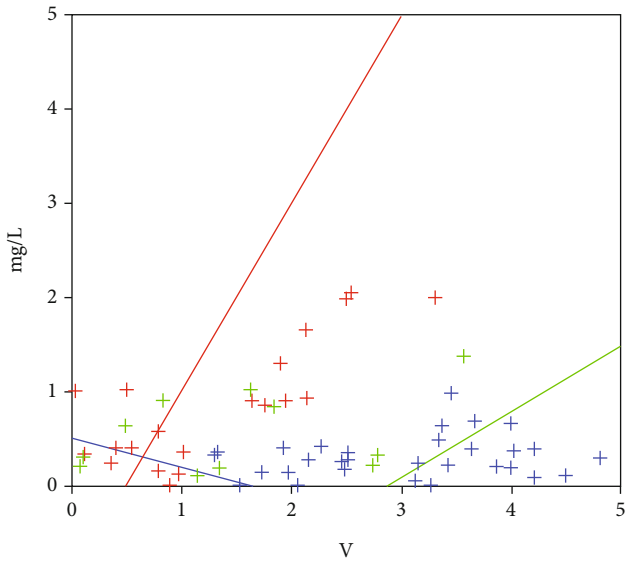

Figure 8: SS significant data.

antispectrophotometric method is selected and the detection range is 0.01 mg/L–0.6 mg/L. After actual testing and related data query, the total phosphorus concentration of the water quality in this water area meets the calibration range, so you can use this method. As shown in Figure 2, it is a spectrophotometer and microwave digestion furnace required for laboratory environment and experiments. The principle of this method is that under acidic conditions, orthophosphate reacts with platinic acid and potassium antimony tartrate to form phosphoplatin heteropoly acid, which is reduced by the reducing agent ascorbic acid to become a blue complex called as phosphoplatin blue. Suspended solid concentration and turbidity are measured by the suspended solid concentration detector and turbidity detector operated and sold by Hangzhou Lucheng Instrument Co. Ltd. The relevant parameters are shown in Table 1, and the instrument is shown in Figure 3.

According to the abovementioned detection methods, the TP, SS, and TUB parameters required for the experiment were detected and a total of 80 sets of measured data were obtained in four experiments.

3.3. Remote Sensing Data and Processing. After reading a large amount of literature and searching and sorting out of the data, it can be found that the Landsat8 satellite is used more frequently in the current satellite water quality remote sensing monitoring research. The Landsat8 satellite was launched by NASA in February 2013. The satellite carries two main payloads, namely, OLI and TIRS. Among them, the OLI land imager contains a total of 9 wavebands, the overall spatial resolution is 30 meters, and the imaging width is 185*185 km. The wavebands and related information of the OL1 land imager are shown in Table 2. The comparison results of different bands can be seen in Figure 4. It can be seen that the band contains the necessary band spectrum information for the three water quality elements discussed in this study. In theory, it can be used for the inversion of the three water quality elements research [30].

Table 2 is reproduced by Ding et al. 2021 (the authors of reference [30] agree to the use of these data in this paper).

The comparison results of different bands can be seen in Figure 4. It can be seen that the band contains the necessary band spectrum information for the three water quality elements discussed in this study. In theory, it can be used for the inversion of the three water quality elements. Moreover, the SWIR1 and SWIR2 bands are significantly different from other bands in the wavelength range and the spatial resolution of the pan band is lower than that of other bands.

The radiometric calibration in this study was performed by the universal calibration tool (radiometric calibration) provided by the ENVI software. The tool first reads the metadata file and calibrates the data into the radiance value (radiance), atmospheric apparent reflectance (reflectance), and brightness temperatures; the conversion formula (1) is as follows:

$$L = \frac{NA}{a} + L_0. \tag{1}$$

This study uses the FLAASH atmospheric correction module provided by ENVI to perform atmospheric correction on Landsat8 images. The FLASH atmospheric correction effect is shown in Figure 5. Generally, after FLASH atmospheric correction is performed, due to the removal of atmospheric influences such as water vapor, the image will become clearer and the color will be more real.

The location of the area studied in this paper is shown by the intersection of the red lines in Figure 5. Because the area of the study is too small, it is difficult to identify. Then, combined with the resolution of landsat8 satellite data and the actual area of East Lake water area, we can find the traditional satellite remote sensing information. The image simply cannot satisfy the research of inversion of water quality elements in small water areas similar to the research object, and it is necessary to obtain higher-resolution remote sensing image data through remote sensing by drones.

4. Proposal of an Inversion Model for Pollutant Concentration in Water Bodies

When a pollution accident occurs, pollutants (organic matter, heavy metals, toxic and hazardous chemicals, etc.) enter the water in a large amount in a short time and follow the general law of pollutant migration, namely, the convection-diffusion equation. Along with the transport process of pollutants in water, there will also be adsorption and analysis processes with the suspended matter, sedimentation and resuspension processes with sediments, chemical reactions, and biodegradation processes. These processes can be used as convection-diffusion equations. The source and sink terms and reaction terms are added to the equation.

$$\frac{\partial C}{\partial t} = \frac{\partial}{\partial x}\left(D_x \frac{\partial C}{\partial x}\right) + \frac{\partial}{\partial y}\left(D_y \frac{\partial C}{\partial y}\right) - \frac{\partial (u_y C)}{\partial x} - \frac{\partial (u_x C)}{\partial y} - KC + R(x, y, t). \tag{2}$$

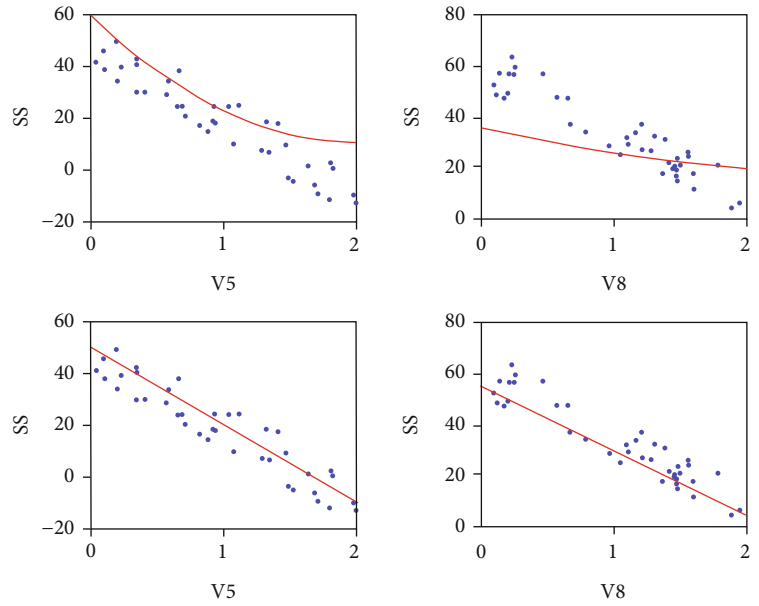

Figure 9: Suspended sediment concentration (SS) inversion model fitting map.

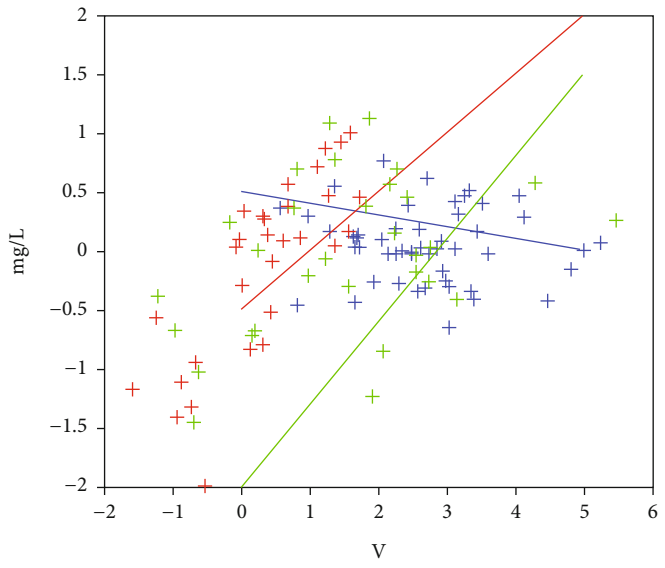

Figure 10: TUB significant data.

Among them, C is the concentration of the pollutant in the water body; Dx and Dy are the diffusion coefficients; u x, uy are the flow velocity components; $R(x, y, t)$ is the source and sink term caused by comprehensive factors; K is the linear reaction coefficient. If you want to further determine the concentration of the pollutant in the water body, you must know the initial concentration distribution of the pollutant in the water body and the concentration distribution law on the water body boundary, that is, the initial conditions and boundary conditions.

Affected by objective factors such as illumination, flight speed, and wind speed, there are some abnormal data in the data, which leads to insufficient correlation of the overall data. Therefore, on the basis of meeting the statistical requirements, draw a scatter plot of the correlation standard data, according to scatter plot to remove abnormal data. First, randomly select 10 groups from the 80 groups of data for testing, add linear trend lines to the scatter plots drawn from the remaining 70 groups of TP data, and judge the most suitable data for fitting according to the edge of the trend line. In Figure 6, the first four spectral parameter data of the trend line from large to small are shown. It can be seen that the trend line $R2$ value of the spectral parameters V5 and V16 is the highest in the scatter plot with TP as the

dependent variable, which are 0.2211 and 0.192, respectively; according to the trend line to remove the abnormal data, the number of remaining samples are nTP = 50.

Taking the optimal spectral parameters V5 and V16 of the remaining samples as independent variables and the corresponding total phosphorus (TP) as the dependent variable, four functional models of the linear regression model, exponential model, power function model, and polynomial model were established using MATLAB software.

The general form of linear function is shown in formula (3):

$$f(x) = mx + b. \tag{3}$$

The general form of the exponential function is shown in formula (4):

$$\begin{aligned} f(x) &= a^x (a > 0, a \neq 1), \\ f(x) &= a^x + mx (a > 0, a \neq 1), \\ f(x) &= ka^x + mx + n (a > 0, a \neq 1). \end{aligned} \tag{4}$$

The general form of the power function is shown in formula (5):

$$\begin{aligned} f(x) &= x^a (a \in R), \\ f(x) &= kx^a + n (a \in R). \end{aligned} \tag{5}$$

The general form of the polynomial function is shown in formula (6):

$$\begin{aligned} Yi &= \beta_0 + \beta_1 X_{1i} + \beta_2 X_{2i} + \cdots + \beta_k X_{ki} + \mu i, \quad (i = 1, 2, \cdots, n), \\ Yi &= \beta_0 + \beta_1 {X_{1i}}^2 + \beta_2 {X_{2i}}^2 + \cdots + \beta_k {X_{ki}}^2 + \mu i, \quad (i = 1, 2, \cdots, n). \end{aligned} \tag{6}$$

The establishment of the four models all come from the curve fitting toolbox of the MATLAB software. The previously processed spectral data is input according to the corresponding data as per the sampling points, and four models are generated, and then, the optimal model is selected according to the correlation coefficient of the model. The model makes predictions.

It can be seen in Figure 7 that the model fitting of four different functions is performed on two different independent variables, and finally, 8 inversion models of total phosphorus (TP) are obtained. According to the determination coefficient of the model, Ra is as large as sorting; we can see that the first four inversion models with larger Ra are PLTri6, UTri6, PTri6, and ETri6 and their coefficients of determination are 0.7965, 0.7963, 0.7948, and 0.7897, respectively. It can be clearly seen that the spectral parameter V16 is used. The fitting of the model has a better fitting effect, and the calculation formula is $RS/R1$, which is the ratio of the near-infrared band to the blue band of the MicaSense RedEdge multispectral sensor. Among them, the polynomial fitting model has the highest coefficient of determination relatively and the overall change trend of the fitting curve shows a general consistency. As the spectral reflectance ratio continues to increase, the total phosphorus (TP) concentration is constantly increasing.

As with the inversion of total phosphorus, affected by objective factors such as illumination, flight speed, and wind speed, there are some abnormal data in the data, which leads to insufficient correlation of the overall data. Therefore, on the basis of meeting the statistical requirements, we randomly selected 10 sample information. After the group inspection data, a scatter plot of the correlation-compliant data is drawn on the 70 sets of SS data born and abnormal data is removed according to the scatter plot. Add a linear trend line to the scatter plot of SS, and judge the data that is most suitable for fitting in the correlation standard data according to the Ra of the trend line. Figure 8 shows the first four spectral parameter data of the trend line from large to small; in the scatter plot with SS as the dependent variable, the trend line Ra value of the spectral parameters V5 and V8 is the highest, RZSS − vs = 0.2884 and RZSS − vs = 0.2459, respectively; abnormal data are removed according to the trend line. The number of remaining samples is $n$ss = 45.

The 8 inversion models of float concentration SS are sorted according to the model's determination coefficient from largest to smallest, as shown in Figure 9. It can be seen that the first four larger inversion models are PLsss, Usss, PLsss, and Usss and their determination coefficients are in order 0.7874, 0.7866, 0.7503, and 0.7467; it can be clearly seen that the spectral parameter V8 used for model fitting has a better fitting effect, and its calculation formula is $(R3 + RS)/R2$, which is the MicaSense RedEdge multispectral sensor. We can get the ratio of the sum of red and near infrared bands to green bands. Among them, the polynomial fitting model has the highest coefficient of determination relatively and the overall change trend of the fitting curve shows a general consistency. As the spectral reflectance continues to increase, the concentration of suspended solids continues to decrease. It can be seen from the trend of each curve that the spectral parameter VS is relatively scattered. Although there is an obvious curve trend and the distribution is more uniform throughout the curve, the spectral parameter V8 is relatively more concentrated in the curve. In the middle part, the distance curve is also more compact, but from the determination coefficient Ra of the model, it can be seen that the two parameters have little difference in the inversion of suspended solid concentration and both can be used as candidates for the inversion of suspended solid concentration.

As with the inversion of total phosphorus, affected by objective factors such as illumination, flight speed, and wind speed, there are some abnormal data in the data, which leads to insufficient correlation of the overall data. After the group inspection data, draw a scatter plot of the correlation-compliant data for the remaining 70 sets of TUB data and remove the abnormal data according to the scatter plot. Add a linear trend line to the scatter plot of TUB and judge the data that is most suitable for fitting in the correlation standard data according to the trend line. In Figure 10, the first four spectral parameter data of the trend line Ra from

large to small are shown. It can be seen that in the scatter plot with TUB as the dependent variable, the trend line Ra value of the spectral parameters V4 and V5 is the highest, 0.3058 and 0.237, respectively; according to the trend line, the abnormal data are removed and the number of remaining samples is 45.

5. Conclusion

At present, the application of satellite remote sensing in the inversion of water quality elements has been basically mature. The inversion model has gradually transitioned from the initial mathematical operation model to the application of the neural network model. Both the inversion method and the inversion accuracy have been achieved. Although we have made some achievements, due to the low resolution of satellite remote sensing images, satellite remote sensing water quality inversion can only be used for large water areas, which has certain limitations for small and micro water areas. Based on the research on the inversion of the concentration of water quality pollutants from satellite remote sensing, this study clarified the spectral information of the bands involved in the inversion of the concentration of water pollution. The inversion of the water quality parameters TP, SS, and TUB obtained good results, providing a new data source and technical means for the water quality monitoring of urban water bodies and providing a reliable basis for the protection and governance of the water environment.

However, there are still many shortcomings and areas that need improvement: (1) the current research on low-altitude UAV water quality remote sensing is still at the basic stage, and there are still some more rigorous methods for acquiring and processing multispectral images. This research failed to achieve the background denoising of multispectral images, which has an impact on the accuracy of the experimental results, which is a limitation. The next step will focus on solving this problem; and (2) this research only solves the experimental problem of remote sensing of water quality by drones, and there is no specific implementation plan for the specific application in the water quality detection system.

5.1. Future Work. The next step can be the detailed study of the water quality monitoring system to specifically solve the problem of water quality monitoring application issues, combining remote sensing of water quality by drones with traditional water quality monitoring methods, to monitor water quality in a planned way.

Data Availability

The data used to support the findings of this study are available from the corresponding author upon request. The authors of reference [30] agree to the use of these data in this paper.

Conflicts of Interest

The authors declare that there is no conflict of interest.

Acknowledgments

The paper was supported by the Natural Science Research Projects in Colleges and Universities of Anhui Province under contract no. KJ2020A0719, Key Project of Research and Development in Chuzhou Science and Technology Program under contract no. 2020ZG016, Open Fund of Hunan Provincial Key Laboratory of Geo-Information Engineering in Surveying, Mapping and Remote Sensing, Hunan University of Science and Technology under contract no. E22136, and Innovation Program for Returned Overseas Chinese Scholars of Anhui Province under contract no. 2021LCX014.

References

[1] S. Helal, J. Li, L. Liu et al., "Predicting academic performance by considering student heterogeneity," *Knowledge-Based Systems*, vol. 161, pp. 134–146, 2018.

[2] K. Bluwstein, M. Buckmann, A. Joseph, S. Kapadia, and Ö. Simsek, "Credit Growth, the Yield Curve and Financial Crisis Prediction: Evidence from a Machine Learning Approach," *SSRN Electronic Journal*, vol. 41, 2021.

[3] F. Guzzetti, S. L. Gariano, S. Peruccacci et al., "Geographical landslide early warning systems," *Earth-Science Reviews*, vol. 200, article 102973, 2020.

[4] K. Chen, H. Chen, C. Zhou et al., "Comparative analysis of surface water quality prediction performance and identification of key water parameters using different machine learning models based on big data," *Water Research*, vol. 171, article 115454, 2020.

[5] S. L. Hyland, M. Faltys, M. Hüser et al., "Early prediction of circulatory failure in the intensive care unit using machine learning," *Nature Medicine*, vol. 26, no. 3, pp. 364–373, 2020.

[6] C. L. Downey, W. Tahir, R. Randell, J. M. Brown, and D. G. Jayne, "Strengths and limitations of early warning scores: a systematic review and narrative synthesis," *International Journal of Nursing Studies*, vol. 76, pp. 106–119, 2017.

[7] J. Berens, K. Schneider, S. Görtz, S. Oster, and J. Burghoff, "Early Detection of Students at Risk–Predicting Student Dropouts Using Administrative Student Data and Machine Learning Methods," *Computer Information*, vol. 12, 2018.

[8] M. S. Tehrany, S. Jones, F. Shabani, F. Martínez-Álvarez, and D. Tien Bui, "A novel ensemble modeling approach for the spatial prediction of tropical forest fire susceptibility using LogitBoost machine learning classifier and multi-source geospatial data," *Theoretical and Applied Climatology*, vol. 137, no. 1-2, pp. 637–653, 2019.

[9] C. Jan, "An effective financial statements fraud detection model for the sustainable development of financial markets: evidence from Taiwan," *Sustainability*, vol. 10, no. 2, p. 513, 2018.

[10] M. Li, H. Xu, and Y. Deng, "Evidential decision tree based on belief Entropy," *Entropy*, vol. 21, no. 9, p. 897, 2019.

[11] Y. Li, W. Jiang, L. Yang, and T. Wu, "On neural networks and learning systems for business computing," *Neurocomputing*, vol. 275, pp. 1150–1159, 2018.

[12] J. C. Quiroz, N. Mariun, M. R. Mehrjou, M. Izadi, N. Misron, and M. A. Mohd Radzi, "Fault detection of broken rotor bar in LS-PMSM using random forests," *Measurement*, vol. 116, pp. 273–280, 2018.

[13] W. F. W. Yaacob, S. A. M. Nasir, W. F. W. Yaacob, and N. M. Sobri, "Supervised data mining approach for predicting student performance," *Indonesian Journal of Electrical Engineering and Computer Science*, vol. 16, no. 3, pp. 1584–1592, 2019.

[14] D. Sun, H. Wen, D. Wang, and J. Xu, "A random forest model of landslide susceptibility mapping based on hyperparameter optimization using Bayes algorithm," *Geomorphology*, vol. 362, article 107201, 2020.

[15] L. T. Vu, N. T. Nguyen, P. Do, T. Th, and D. P. Dao, "Feature selection methods and sampling techniques to financial distress prediction for Vietnamese listed companies," *Investment Management and Financial Innovations*, vol. 16, no. 1, pp. 276–290, 2019.

[16] M. F. Ijaz, G. Alfian, M. Syafrudin, and J. Rhee, "Hybrid prediction model for type 2 diabetes and hypertension using DBSCAN-based outlier detection, synthetic minority over sampling technique (SMOTE), and random forest," *Applied Sciences*, vol. 8, no. 8, p. 1325, 2018.

[17] Y. Abuov and O. Omirtay, "BIM-GIS technologies in analysing the cost of assets after natural disasters: water flood and earthquake," in *International Scientific and Practical Conference" Geosystemic approach to the study of the natural environment of the Republic of Kazakhstan*, Zambia, 2018.

[18] M. AlHamaydeh, G. Al-Shamsi, N. Aly, and T. Ali, "Geographic information system-based seismic risk assessment for Dubai, UAE: a step toward resilience and preparedness," *Practice Periodical on Structural Design and Construction*, vol. 27, no. 1, article 04021069, 2022.

[19] Z. I. Andromeda, C. Randi, K. Nazhifah, R. Syahputra, and M. R. Septyandy, "Efforts to improve community awareness towards the potential of a great earthquake which threats Jakarta based on geographic information and 3D simulation systems in Matraman district, East Jakarta," *IOP Conference Series: Earth and Environmental Science*, vol. 279, no. 1, article 012004, 2019.

[20] Y. Ban, H. Liu, and J. Yuan, "Design and development of an earthquake emergency coordinating consultation system Based on GIS," in *2019 2nd International Conference on Safety Produce Informatization (IICSPI)*, pp. 231–234, IEEE, Chongqing, China, 2019.

[21] J. Briones-Bitar, P. Carrión-Mero, N. Montalván-Burbano, and F. Morante-Carballo, "Rockfall research: a bibliometric analysis and future trends," *Geosciences*, vol. 10, no. 10, p. 403, 2020.

[22] G. P. Chen, J. S. Zhao, L. Yuan, Z. J. Ke, M. Gu, and T. Wang, "Implementation of a geological disaster monitoring and early warning system based on multi-source spatial data: a case study of Deqin county, Yunnan province," *Natural Hazards and Earth System Sciences Discussions*, vol. 41, pp. 1–15, 2017.

[23] X. Chen, D. Jia, and W. Zhang, "Integrating UAV Photogrammetry and Terrestrial Laser Scanning for Three-Dimensional Geometrical Modeling of Post-Earthquake County of Beichuan," in *International Conference on Computing in Civil and Building Engineering*, pp. 1086–1098, Springer, Cham, 2021.

[24] Y. Chen, X. Zeng, and T. Yuan, "Design and Development of Earthquake Emergency Rescue Command System Based on Gis and Gps," in *International Symposium for Intelligent Transportation and Smart City*, pp. 126–138, Springer, Singapore, 2017.

[25] J. Dou, A. P. Yunus, D. Tien Bui et al., "Evaluating GIS-based multiple statistical models and data mining for earthquake and rainfall-induced landslide susceptibility using the LiDAR DEM," *Remote Sensing*, vol. 11, no. 6, p. 638, 2019.

[26] S. Giovinazzi, C. Marchili, A. Di Pietro et al., "Assessing earthquake impacts and monitoring resilience of historic areas: methods for GIS tools," *ISPRS International Journal of Geo-Information*, vol. 10, no. 7, p. 461, 2021.

[27] V. G. Gitis and A. B. Derendyaev, "Web-Based GIS Platform for Automatic Prediction of Earthquakes," in *International Conference on Computational Science and Its Applications*, pp. 268–283, Springer, Cham, 2018.

[28] R. Guardo, L. De Siena, and C. Dreidemie, "Mt. Etna feeding system and sliding flank: a new 3D image from earthquakes distribution in a customisable GIS," *Earth Science*, vol. 8, p. 474, 2020.

[29] Z. Han, F. Yang, Y. Li et al., "GIS-based three-dimensional SPH simulation for the 11 April 2018 Yabakei landslide at Oita Nakatsu, Japan," *Water*, vol. 13, no. 21, p. 3012, 2021.

[30] C. Ding, X. Zhang, S. Ma, W. Han, Y. Lu, and J. Yin, "Estuary water quality classification through deep learning image segmentation, an example of Hangzhou Bay," in *2021 9th International Conference on Agro-Geoinformatics (Agro-Geoinformatics)*, Shenzhen, China, 2021.